

Broad and Luminous [OIII] and [NII] in Globular Cluster ULXs

R.L. Porter*

Department of Astronomy, University of Michigan, 500 Church Street, Ann Arbor, MI, 48109-1042, USA

Received

ABSTRACT

We consider an accretion-disc origin for the broad and luminous forbidden-line emission observed in ultraluminous X-ray (ULX) sources CXOJ033831.8-352604 and XMMU 122939.7+075333 in globular clusters hosted by elliptical galaxies NGC 1399 and NGC 4472, respectively. We will refer to the latter by the globular cluster name RZ2109. The first has strong [OIII] and [NII], the second only [OIII]. Both $H\alpha$ and $H\beta$ are very weak or undetected in both objects. We assume that the large line widths are due to Keplerian rotation around a compact object and derive expressions for maximum line luminosities. These idealized models require central masses $\gtrsim 100$ and $\gtrsim 30000 M_{\odot}$ for CXOJ033831.8-352604 and RZ2109, respectively. An independent, bootstrap argument for the total disc mass yields, for both systems, $M_{\text{disc}} \gtrsim 10^{-4} M_{\odot}$ for a purely metallic disc (and two orders of magnitude larger for solar metallicities). If Roche-lobe overflow is implicated, viscous time-scales are $\gtrsim 300$ yr. Standard disc theory then offers another limit on the central masses. Lobe radii for a $\sim 1 M_{\odot}$ donor are $\gtrsim 10^{13}$ cm. We therefore rule out Roche-lobe overflow of a white dwarf in both systems. Red giants could fill the necessary lobes. Whether they are too metal-poor to produce the strong forbidden lines without strong hydrogen emission is unclear.

Key words: galaxies: individual (NGC 1399) – galaxies: individual (NGC 4472) – galaxies: star clusters – accretion, accretion discs.

1 INTRODUCTION

Ultraluminous X-ray sources are point sources that appear to exceed the Eddington luminosities of stellar-mass compact objects. They are therefore prime candidates for long-sought intermediate-mass black holes (IMBHs). ULXs have been studied extensively since their discovery in the early 1980s, and they continue to be the subjects of intense research activity (Miller, Fabian, & Miller 2004; Winter, Mushotzky, & Reynolds 2006; Hui & Krolik 2008; King 2008, 2009).

Zepf et al. (2007; 2008, hereafter Z08) and Irwin et al. (2010, hereafter I10) recently identified very broad and luminous [OIII] $\lambda 5007$ emission in two ULXs harbored by globular clusters in elliptical galaxies NGC 4472 and NGC 1399, respectively. The connections to globular clusters are robust, as in both I10 and Z08, we see large redshifts that agree very well with the redshifts of the clusters and their host galaxies. Line widths were 140 and 1500 km s⁻¹ in the two systems, and line luminosities, assuming the sources radiate isotropically, were 10^{36-37} erg s⁻¹. Both Z08 and I10 found difficulty simultaneously explaining the line widths and luminosities with an accretion disc around a stellar black hole, the most natural explanation for a consistent source with $L_x \approx 10^{39}$ erg s⁻¹. The observed lines created a tension. Their large line widths suggested rapid rotation very close to the source, while the large luminosities suggested a large line-emitting region and an

origin in the outer disc. The lack of $H\alpha$ and $H\beta$ presented further complications in the context of globular clusters. Z08 suggested a stellar black-hole wind is the explanation for RZ2109. I10 suggested for CXOJ033831.8-352604 tidal disruption of a white dwarf by an IMBH (Fabian, Pringle, & Rees 1975; Rosswog, Ramirez-Ruiz, & Hix 2009).

This Letter is organized as follows. In section 2, we revisit and extend the arguments presented by Z08 and I10, first relaxing the assumption that the line-emitting gas cannot be more dense than the critical density of the observed lines. We derive a simple expression for the maximum line luminosity in an accretion-disc geometry. Our expression is independent of temperature, density, and metallicity, and depends only on rotational velocity and central mass. While a super-critical density alleviates some of the tension described above, we nonetheless confirm the Z08 and I10 conclusions that stellar-mass accretion cannot be implicated in either ULX. In section 3, we present bootstrap arguments for the total mass in an accretion disc and obtain lower limits. In section 4, we explore the implications for Roche-lobe overflow.

2 MAXIMUM LINE LUMINOSITIES

Here we derive expressions for the maximum line luminosities of the [OIII] and [NII] forbidden lines. We focus on the [OIII] lines because they are seen in both objects. Because both [NII] and [OIII] are produced by ions of the carbon isoelectronic sequence,

* E-mail: rlporter@umich.edu

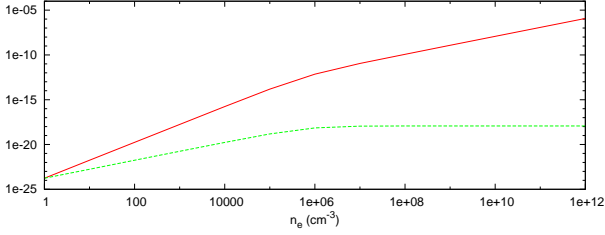


Figure 1. [OIII] $\lambda 5007$ emissivity (red solid, $\text{erg cm}^{-3} \text{s}^{-1}$) and intensity (green dashed, $\text{erg cm}^{-2} \text{s}^{-1}$) emitted in an isothermal, constant-density line-of-sight with solar metallicity and column density 1 cm^{-2} . Each curve is a function of volume density. The critical density can be seen as a “knee” in each curve near $n_e = 10^6 \text{ cm}^{-3}$.

our formalism applies to both. The final expression is independent of temperature, density, and metallicity and depends only on rotational velocity and central mass.

We assume the gas is photoionized and collisionally excited and begin by writing a simple two-level balance equation

$$n_e n_1 q_{12} = n_e n_2 q_{21} + n_2 A_{21}, \quad (1)$$

where n_1 and n_2 are the populations of the lower and upper levels, A_{21} is the spontaneous radiative transition probability (s^{-1}) from level 2 to level 1, and q_{12} and q_{21} are the collisional excitation and de-excitation coefficients ($\text{cm}^3 \text{s}^{-1}$) and are related by $q_{12} = \frac{\omega_2}{\omega_1} q_{21} \exp(-h\nu/kT)$. The critical density $n_{\text{crit}} \equiv A_{21}/q_{21}$ is the density at which the collisional de-excitation rate ($n_e q_{21}$) equals the radiative decay rate. For $n_e \ll n_{\text{crit}}$, the radiative decay dominates and the population of level 2 is

$$n_2 = \frac{n_e n_1 q_{12}}{A_{21}}. \quad (2)$$

For $n_e \gg n_{\text{crit}}$, the usual Boltzmann equation of local thermodynamic equilibrium (LTE) applies. The local emissivity is $\epsilon = n_2 h\nu_{21} A_{21}$, and it follows that

$$\epsilon = \begin{cases} n_e n_1 q_{12} h\nu_{21} & n_e \ll n_{\text{crit}} \\ n_1 \frac{\omega_2}{\omega_1} \exp(-h\nu/kT) h\nu_{21} A_{21} & n_e \gg n_{\text{crit}}. \end{cases} \quad (3)$$

The critical density marks the transition from the regime where radiative cooling is proportional to $n_e n_{\text{ion}}$ to the LTE regime where cooling is proportional to n_{ion} . The emitted energy per unit volume per unit time increases monotonically with increasing density. The two regimes are illustrated in Figure 1 for the [OIII] $\lambda 5007$ line. The critical density is represented by the knee near 10^6 cm^{-3} .

Both I10 and Z08 considered the low-density case, and we have no need to reconsider that here. The remainder of this work will assume $n_e > n_{\text{crit}}$. Authors who have discussed the high-density behavior of [OIII] emission include Nussbaumer & Storey (1981), Keenan & Aggarwal (1987), Kastner & Bhatia (1989), and Osterbrock & Ferland (2006). From an observational perspective, we note, for example, Andreä, Dreschel, & Starrfield (1994) found n_e as high as 10^8 cm^{-3} from [OIII] lines in classical novae.

We generalize the high-density emissivity to multi-level configurations by using the O^{+2} calculations of Nussbaumer & Storey (1981). Their calculations are valid for all practical densities and include temperatures as high 40,000 K, safely above the temperature of photoionized O^{+2} gas considered in section 3 below. The upper level of the [OIII] $\lambda 5007$ and [NII] $\lambda 6548$ transitions is 1D_2 . The fractional population $f(^1D_2)$ in Table 5 of Nussbaumer & Storey

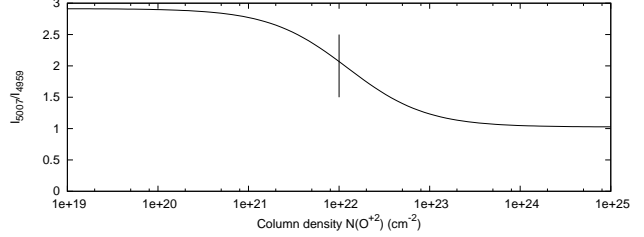


Figure 2. Theoretical ratio of the lines in the [OIII] doublet $\lambda\lambda 4959, 5007$ as a function of O^{+2} column density. Observations in both Z08 and I10 clearly suggest ratios toward the canonical optically-thin value. The vertical bar marks $N(\text{O}^{+2}) = 10^{22} \text{ cm}^{-2}$ (or $\tau_{5007} = 1$).

does not exceed ≈ 0.2 . A comparable value applies to N^+ , and our emissivities take the maximum value

$$\epsilon_{\text{max}} = n_A f(^1D_2)_{\text{max}} h\nu_{21} A_{21}, \quad (4)$$

where n_A is the density of the ionization stage.

Next we posit a column of gas having local emissivity given by Equation 4. The intensity emitted through the column is

$$I_\lambda = \int \epsilon dz, \quad (5)$$

where z represents position along the column (or above an annulus perpendicular to the plane of the accretion disc). To impose an upper limit on the integration variable, we introduce a photon escape probability, $P_{\text{esc}} = \frac{1}{1+\tau}$, where τ is the (Napier) line-center optical depth. Equation 5 is then written

$$I_\lambda^{\text{max}} = N_A f(^1D_2)_{\text{max}} h\nu_{21} A_{21} P_{\text{esc}}, \quad (6)$$

where we have used $N_A = n_A \int dz$.

Equation 6 saturates at $\tau \approx 1$, consistent with the rule-of-thumb that we can see into a cloud only up to optical depth unity (e.g., Rybicki & Lightman 1979). The upper limit corresponds to $N(\text{O}^{+2}) \approx 10^{22} \text{ cm}^{-2}$, assuming local line widths are thermal at $\approx 10^4 \text{ K}$. Optical depth in the [OIII] lines causes their relative strengths to decrease from the canonical 3:1 ratio to approximate parity in the optically-thick limit. This behavior is shown in Figure 2. The plotted ratio is visibly greater than unity in both Z08 and I10. Our limit, therefore, has the consequence of preventing model line-ratios inconsistent with the observations.

Note that Equation 6 does not depend upon density. The green dashed curve in Figure 1 illustrates this and is an important point in our analysis. Above the critical density, the intensity emitted through a fixed column density is independent of the volume density of the gas. This means that, with no penalty on the total intensity, we can increase the density and, with all else fixed, squeeze the gas into a smaller volume, potentially allowing a stellar-mass black hole explanation.

Finally, we obtain a maximum luminosity via an effective surface area. We define the inner radius, r_0 , of our line-emitting region by assuming the line-emitting gas is in a Keplerian orbit about central mass M with velocity v (which we relate to observed line-widths below) so that

$$r_0 = GM/v^2. \quad (7)$$

We assume the line-emitting region comprises an annulus with width comparable to r_0 . Line luminosities are written

$$L_\lambda = 4\pi r_0^2 I_\lambda = 4\pi \left(\frac{GM}{v^2} \right)^2 I_\lambda. \quad (8)$$

Table 1. Observed and model luminosities (erg s^{-1}). The last column contains the L_{λ}^0 values defined via equation 9.

Quantity	CXOJ033831.8-352604	RZ2109	L_{λ}^0
L_{5007}	$\text{few} \times 10^{36}$	1.4×10^{37}	2.4×10^{33}
L_{6584}	3×10^{36}	unobs.	2.8×10^{32}
L_x	$1.5 - 2.3 \times 10^{39}$	4×10^{39}	

We evaluate constants, normalize variables to convenient values, and obtain maximum luminosity

$$L_{\lambda}^{\text{max}} = L_{\lambda}^0 M_1^2 v_{100}^{-4}. \quad (9)$$

where M_1 is the central mass in units M_{\odot} , v_{100} is the rotational velocity in units 100 km s^{-1} , and all constants have been absorbed into fiducial values L_{λ}^0 . Table 1 contains the fiducial luminosities for [OIII] $\lambda 5007$ and [NII] $\lambda 6584$. Atomic data used in this section are from Wiese, Fuhr, & Deters (1996), as obtained from the NIST Atomic Spectra Database (Ralchenko et al. 2008).

It is important to emphasize that equations 8 and 9 are independent of temperature, volume density, and metallicity. This is by design. However, temperature and metallicity do inform the *practicality* of the equations. We will discuss the former below. Regarding the latter, at fixed n_e , the disc height required to reach a certain column density (and therefore luminosity) is inversely proportional to metallicity. A purely metallic plasma allows the smallest disc height for the maximum-luminosity configuration of our model. Solar metallicity gas requires a disc height more than three orders of magnitude greater, reaching ≈ 10 Thomson depths. Scattering would yield emergent line widths $\sim 1000 \text{ km s}^{-1}$. Such large widths would contradict our rotational broadening assumption in both ULXs and are ruled out completely by observation in CXOJ033831.8-352604. If the width scales as the number of scatterings (usually the greater of τ and τ^2), this problem would be eliminated by decreasing the column by some factor. The minimum central mass found below would increase by the square of that factor.

We plot in Figure 3 maximum line luminosities as a function of the velocity of the gas at r_0 . Several values of the compact object mass are considered. The middle two lines represent recent theoretical ($80 M_{\odot}$) and observed ($30 M_{\odot}$) upper limits to the mass of a stellar black hole (Belczynski et al. 2010). Results for I10 and Z08 are indicated by the squares, where we have assumed velocities equal to $1/(2\sqrt{\ln 2})$ times the measured FWHM. This ignores the effect of disc inclination on the observed line widths. Accounting for inclination would mean a greater rotational velocity and a smaller annulus radius (for a given central mass). This would decrease the surface area of the line-emitting region and the luminosity of the line. The arrow on each square points to the velocity appropriate for the (arbitrarily chosen) inclination angle 45° .

The point corresponding to CXOJ033831.8-352604 in the upper panel of Figure 3 is beneath the lines corresponding to the theoretical and observed stellar-mass black hole upper limits. However, the lower panel of Figure 3 makes a more compelling case. The observed L_{6584} is very slightly less than (at edge-on inclination) the maximum predicted luminosity corresponding to the maximum theoretical mass of a stellar black-hole (Belczynski et al. 2010). Note that these predictions assume optimal cooling efficiency. I10 found $T_e \leq 13,000 \text{ K}$ in the [NII] emitting region using the lack of $\lambda 5755$. Using this temperature would lower the [NII] predictions by a factor ~ 2 and require $M \gtrsim 100 M_{\odot}$. [OIII] $\lambda 4363$ was neither

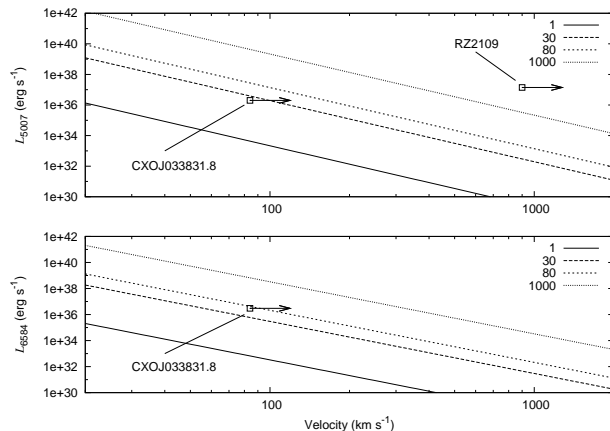


Figure 3. Maximum line luminosities (upper: [OIII] $\lambda 5007$; lower: [NII] $\lambda 6584$) versus rotational velocity of the line-emitting region for several values of the central mass (in units M_{\odot}). Squares indicate results from I10 and Z08. Arrows point from minimum (edge-on) velocity to the velocity appropriate for 45° inclination. [NII] was not detected in RZ2109.

presented nor mentioned in I10. Measurement of this line could place a strong constraint on the temperature of the [OIII] region.

The upper panel of Figure 3 clearly demonstrates that the Z08 observations of RZ2109 cannot be explained as Keplerian rotation around a stellar-mass object. The required mass is at least $6000 M_{\odot}$. [OIII] $\lambda 4363$ is weakly detected in RZ2109. A rough estimate is that $\lambda 5007$ is at least 10 times greater. The Nussbaumer & Storey (1981) tabulations would then give $T \lesssim 15,000 \text{ K}$ at the $\lambda 5007$ critical density. That upper limit quickly decreases to $T \lesssim 7,500 \text{ K}$ for $n_e \gtrsim 10^7 \text{ cm}^{-3}$. These considerations depress the maximum luminosity by at least a factor of 20, so that the minimum central mass is at least $30,000 M_{\odot}$.

We rule out stellar black-hole Keplerian accretors in both sources. Sub-Keplerian motions have orbiting radii that are smaller for a given central mass than Keplerian, decreasing the surface area of the line-emitting region and exacerbating the problems discussed above. We can therefore rule out sub-Keplerian, stellar black hole accretion more readily than we can rule out Keplerian.

We stress that the two panels of Figure 3 do not depend upon the relative abundances of oxygen and nitrogen. The predicted [NII] luminosities are noticeably less than the [OIII] luminosities at the same velocity and central mass. This is because the [NII] lines are less efficient coolants than their [OIII] counterparts.

3 TOTAL DISC MASS

Here we present a bootstrap argument for the total disc masses in an accretion scenario. The mass required to emit L_{5007} (or L_{6584}) is

$$M(^1D_2) = \frac{Zm_p L_{\lambda}}{hvA}, \quad (10)$$

where Zm_p is the mass of a single atom with mass number Z . This is independent of the geometrical model and the gas density (even below n_{crit}), and accounts only for the population in the upper level of the transition. Observed values of L_{λ} are listed in Table 1. The [OIII] lines require masses $\sim 3 \times 10^{-7}$ and $\sim 2 \times 10^{-6} M_{\odot}$ for CXOJ033831.8-352604 and RZ2109, respectively. The [NII] lines in CXOJ033831.8-352604 require $4 \sim 10^{-6} M_{\odot}$.

We can bootstrap our way to a total disc mass via

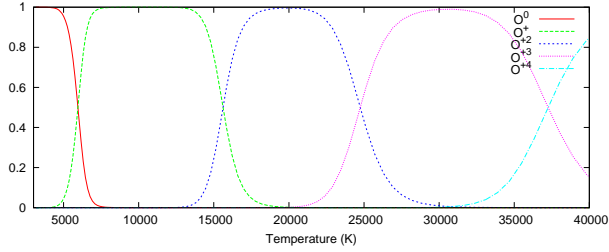


Figure 4. Ionization fractions of oxygen as a function of the temperature of an intense blackbody.

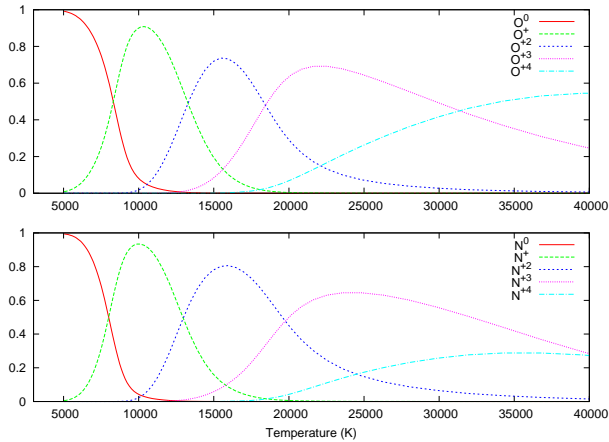


Figure 5. Ionization fractions of oxygen (upper panel) and nitrogen (lower panel) as a function of the electron temperature of gas ionized by a power-law continuum with spectral index $\Gamma = 2.5$.

$$\frac{M(^1D_2)}{M_{\text{disc}}} = \frac{\rho_Z}{\rho} \frac{\int f_{\text{ion}} f(^1D_2) r dr}{\int r dr}, \quad (11)$$

where $f(^1D_2)$ was discussed in section 2 and f_{ion} is the C-like ionization fraction, which we estimate using the well-known plasma simulation code Cloudy (version C08, last described by Ferland et al. 1998). Figure 4 plots the results for oxygen as a function of the temperature of a bright blackbody photoionization source. The fraction in O^{+2} peaks around 20,000 K. The maximum equivalent width of $\lambda 5007$ with $N(\text{O}^{+2}) = 10^{22} \text{ cm}^{-2}$ against a blackbody of the same area and $T_{\text{BB}} = 20,000 \text{ K}$ is about 1 \AA . We estimate from spectra in I10 and Z08 observed equivalent widths of 5 and 15 \AA . Blackbody sources with weak enough continuum at $\sim 5000 \text{ \AA}$ are too weak to ionize O^+ . We require a harder continuum.

We instead consider, again using Cloudy, a power-law continuum with spectral index $\Gamma = 2.5$ (following X-ray continuum fits in I10). Figure 5 plots both oxygen and nitrogen ionization fractions as a function of electron temperature. The ionization parameter ranges from $-9 \leq \log U \leq 0$.

The fractions f_{ion} and $f(^1D_2)$ depend on temperature. We relate them to the variable of integration r via the standard Shakura-Sunyaev prescription ($T \propto r^{-3/4}$). The ratio of integrals in equation 11 is illustrated by the dotted blue curves in Figure 6. The result depends on the upper limit of integration. The peak is $\approx 4\%$ for both oxygen and nitrogen. The curves decline as r^{-2} at large radii.

An important conclusion can be derived from Figures 5 and 6. The regions emitting [OIII] and [NII] are mostly non-cospatial. The details depend on the ionizing source and the geometry. Since

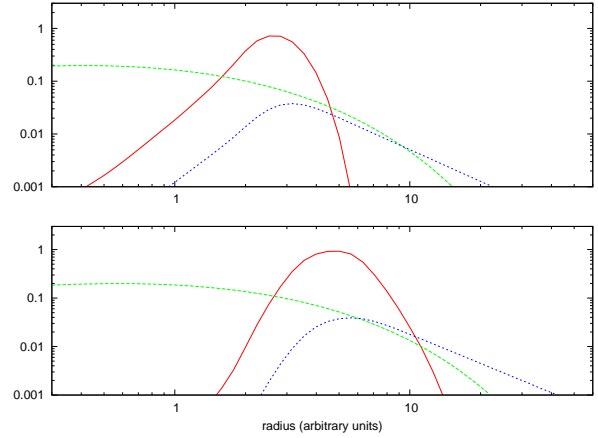


Figure 6. Level and ionization stage fractions of oxygen (upper panel) and nitrogen (lower panel) versus normalized radius. Solid red lines are fractions in O^{+2} and N^+ , dashed green lines are $f(^1D_2)$, and dotted blue lines are ratios of integrals given in the right-hand side of equation 11.

the second ionization energy of nitrogen is only 85% of the second ionization energy of oxygen, the basic result is fairly robust. N^+ always peaks at a temperature significantly less than the temperature of the O^{+2} peak. If the standard α -disc is applicable, we have $T \propto r^{-3/4}$. Keplerian rotation gives $v \propto r^{-1/2}$, so $v \propto T^{2/3}$. A series of tests suggests the [OIII] and [NII] line widths should differ by a factor $\gtrsim 1.4$. The widths are uncertain but appear comparable in the I10 observations. This argues against Keplerian rotation about *any* central mass in CXOJ033831.8-352604. A very steep temperature gradient or a thermal instability between the [OIII] and [NII] regions could mitigate this problem. High-resolution spectroscopy would be useful in efforts to address such questions.

Finally, we require the density of oxygen relative to the total gas density. Assuming metallicity is independent of radius, we can write

$$\frac{\rho_Z}{\rho} = \frac{A n_Z}{\sum A n_Z} \quad (12)$$

where A is atomic mass number. For fixed relative metal abundances, the fraction of mass in oxygen varies from ~ 0.005 with solar abundances (Grevesse & Sauval 1998) to ~ 0.4 for all metals.

Combining the above results, we find $M_{\text{disc}} \gtrsim 10^{-4} M_{\odot}$. This corresponds to the purely metallic case. If we assume roughly solar abundances, $M_{\text{disc}} \gtrsim 10^{-2} M_{\odot}$. An estimate for the upper limit is not readily apparent in either system because we have no way of estimating the outer radius and, in particular, because the line-emitting gas could be only a thin outermost layer of the disc.

4 ROCHE-LOBE OVERFLOW

In steady Roche-lobe overflow accretion, the disc mass must be replenished on the viscous time-scale

$$t_{\text{visc}} = \frac{M_{\text{disc}}}{\dot{M}}, \quad (13)$$

where the mass-accretion rate $\dot{M} = L_x/\eta c^2$ and η is an efficiency typically taken to be 0.1. We can also consider the viscous time-scale in a standard α -disc. We manipulate the familiar expression (Frank, King, & Raine 2002), substituting azimuthal velocity for the radius via equation 7, and obtain

$$t_{\text{visc}} \approx 4.2\alpha^{-4/5} \dot{M}_{16}^{-3/10} M_1^{3/2} v_{100}^{-5/2} \text{ yr}, \quad (14)$$

where \dot{M}_{16} is the mass accretion rate in units 10^{16} g s^{-1} . For the X-ray luminosities given in Table 1, we find $\dot{M} \approx 2 \times 10^{19} \text{ g s}^{-1}$ ($3 \times 10^{-7} M_{\odot} \text{ yr}^{-1}$).

If we assume the ‘‘edge-on’’ velocities discussed in relation to Figure 3 and $\alpha = 0.1$, equations 13 and 14 require masses 70 and $4000 M_{\odot}$ for CXOJ033831.8-352604 and RZ2109, respectively. These numbers are surprisingly similar to the minimum masses found in Section 2. The minimum masses are ~ 40 times larger if the disc has $Z \approx 0.3Z_{\odot}$. The viscous time-scale $t_{\text{visc}} \gtrsim 300 \text{ yr}$.

Temperatures derived with the α -disc prescription, standard assumptions, and the above limits are too cold by a factor ~ 10 . M_1 , \dot{M} , and α all enter as fairly weak powers and offer no obvious solution. Irradiation of a surface layer (e.g., Dubus et al. 1999) might yield the necessary temperatures.

Can a globular cluster form and sustain the massive accretion discs implied by the observed [OIII] luminosities? Combining the minimum masses obtained in Section 2 with the rotational velocities derived above, we obtain $r_0 \approx 2 \times 10^{14}$ and $5 \times 10^{14} \text{ cm}$, for CXOJ033831.8-352604 and RZ2109, respectively. We take this as the distance from the center of the compact object to the Lagrange point L_1 . We then assume a $1 M_{\odot}$ donor star (giving mass ratios $q = 0.01$ and 1.7×10^{-4}) and employ approximations from Eggleton (1983) and Frank, King & Raine (2002), and we obtain donor Roche lobe radii $r_L \gtrsim 10^{13}$ and $5 \times 10^{12} \text{ cm}$, respectively. These radii are comfortably within the size limits of the red giants that are common in globular clusters, but they represent lower limits. Larger central object masses would correspond to larger overflow radii (because the dependence of r_L/r_0 on M via q is not enough to overcome $r_0 \propto M$). White dwarfs have been mentioned because of the apparent high-metallicity in both systems. With prototypical $M_{wd} = 0.6 M_{\odot}$ and $r_{wd} = 10^9 \text{ cm}$, we can *strongly* exclude white dwarfs as Roche-lobe overflow donors in either system.

Does the envelope of a red giant contain enough oxygen to produce the observed line luminosities? Carretta & Gratton (1997) considered the metallicities of red giants in 24 galactic globular clusters. They found sub-solar metallicities for every star in their study. The majority were sub-solar by at least an order of magnitude. The most metal-rich had $Z \approx 0.3Z_{\odot}$.

The [OIII]/H β and [NII]/H α values I10 observed in CXOJ033831.8-352604 ($\gtrsim 5$ and $\gtrsim 7$, respectively) and the [OIII]/H β value Z08 observed in RZ2109 (~ 30) are not necessarily indicative of high-metallicity gas. The photoionized gas near the center of the giant HII region 30 Doradus has $Z \approx 0.3Z_{\odot}$ and [OIII]/H $\beta \approx 6$ (Pellegrini et al., submitted). Elevated ratios are often thought to be signs of radiative shock heating (e.g., Dopita & Sutherland 1995), as was noted by Z08. Detailed attempts to distinguish between enhanced abundances and non-equilibrium heating processes are probably unwarranted without better observational constraints. A further complication pertains to whether the line-emitting gas is radiation- or matter-bound (McCall, Rybski, & Shields 1985), although the high observed [NII]/H α would seem to make the latter less likely in CXOJ033831.8-352604.

If Z08 are correct in their black-hole wind explanation of RZ2109, we offer without comment the suggestion that the observed very broad line-widths may be the low-resolution appearance of narrow emission lines atop broader ones as in a two-wind structure (e.g., Fernandes 1999).

5 ACKNOWLEDGMENTS

RLP thanks referee John Raymond for excellent suggestions and criticisms and Joel Bregman, Gary Ferland, Jimmy Irwin, Jon Miller, Eric Pellegrini, Mark Reynolds, and Pete Storey for fruitful discussions.

REFERENCES

- Andr a J., Dreschel H., Starrfield S., 1994, A&A, 291, 869
 Belczynski K., Bulik T., Fryer C. L., Ruitter A., Valsecchi F., Vink J. S., Hurley J. R. 2010, ApJ, 714, 1217
 Carretta E., Gratton R. G. 1997, A&AS, 121, 95
 Dopita M. A., Sutherland R. S., 1995, ApJ, 455, 468
 Dubus G., Lasota J.-P., Hameury J.-M., Charles P., 1999, MNRAS, 303, 139
 Eggleton P., 1983, ApJ, 268, 368
 Fabian A. C., Pringle J. E., Rees M. J. 1975, MNRAS, 172, 15
 Ferland G. J., Korista K. T., Verner D. A., Ferguson J. W., Kingdon J. B., Verner E. M. 1998, PASP, 110, 761
 Fernandes R. C., Jr. 1999, MNRAS, 305, 602
 Frank J., King A., Raine D., 2002, Accretion Power in Astrophysics, 3rd. ed. Cambridge, UK: Cambridge University Press
 Grevesse N., Sauval A., 1998, Space Science Reviews, 85, 161
 Hui Y., Krolik J., 2008, ApJ, 679, 1405
 Jos e J., Hernanz M., 1998, ApJ, 494, 680
 Kastner S. O., Bhatia A. K., 1989, ApJSS, 71, 665
 Keenan F. P., Aggarwal, K. M. 1987, ApJ, 319, 403
 King A. R., 2008, MNRAS, 385, 113
 King A. R., 2009, MNRAS, 393, 41
 Irwin J. A., Brink T. G., Bregman J. N., Roberts T. P., 2010, ApJ, 712, 1
 McCall M. L., Rybski P. M., Shields G. A., 1985, ApJS, 57, 1
 Miller J. M., Fabian A. C., Miller M. C., 2004, ApJ, 614, 117
 Nussbaumer H., Storey P. J., 1981, A&A, 99, 177
 Osterbrock D. E., Ferland G. J., 2006, Astrophysics of gaseous nebulae and active galactic nuclei, 2nd. ed. by D.E. Osterbrock and G.J. Ferland. Sausalito, CA: University Science Books
 Pellegrini E. et al., submitted
 Ralchenko Yu., Kramida A. E., Reader J., NIST ASD Team (2008). NIST Atomic Spectra Database (version 3.1.5), [Online]. Available: <http://physics.nist.gov/asd3> [2010, March 29]. National Institute of Standards and Technology, Gaithersburg, MD.
 Rosswog S., Ramirez-Ruiz E., Hix W. R. 2009, ApJ, 695, 404
 Rybicki G. B., Lightman A., 1979, Radiative Processes in Astrophysics, New York, Wiley.
 Shakura N. I., Sunyaev R. A., 1973, A&A, 24, 337
 Wiese W. L., Fuhr J. R., Deters T. M., 1996, J. Phys. Chem. Ref. Data, Monograph No. 7
 Winter L. M., Mushotzky R. F., Reynolds C. S., 2006, 649, 730
 Zepf S. E., Maccarone T. J., Bergond G., Kundu A., Rhode K. L., Salzer J. J., 2007, ApJ, 669, 69
 Zepf S. E., Stern D., Maccarone T. J. et al., 2008, ApJ, 683, 139

This paper has been typeset from a $\text{\TeX}/\text{\LaTeX}$ file prepared by the author.